Journal of Biomedical Optics

SPIEDigitalLibrary.org/jbo

Functional photoacoustic microscopy of pH

Muhammad Rameez Chatni
Junjie Yao
Amos Danielli
Christopher P. Favazza
Konstantin I. Maslov
Lihong V. Wang

Functional photoacoustic microscopy of pH

Muhammad Rameez Chatni, Junjie Yao, Amos Danielli, Christopher P. Favazza, Konstantin I. Maslov, and Lihong V. Wang
Washington University in St. Louis, Optical Imaging Laboratory, Department of Biomedical Engineering, One Brookings Drive, St. Louis, Missouri 63130

Abstract. pH is a tightly regulated indicator of metabolic activity. In mammalian systems, an imbalance of pH regulation may result from or result in serious illness. In this paper, we report photoacoustic microscopy (PAM) of a commercially available pH-sensitive fluorescent dye (SNARF-5F carboxylic acid) in tissue phantoms. We demonstrated that PAM is capable of pH imaging in absolute values at tissue depths of up to 2.0 mm, greater than possible with other forms of optical microscopy. [DOI: 10.1117/1.3644495]

Keywords: photoacoustic microscopy; pH imaging; SNARF-5F carboxylic acid.

Paper 11186LRR received Apr. 12, 2011; revised manuscript received Aug. 24, 2011; accepted for publication Sep. 9, 2011; published online Oct. 14, 2011.

pH regulation provides distinct environmental conditions for metabolic pathways, and for energy storage in the form of electrochemical potential gradients in cells. Additionally, almost all proteins depend on pH to maintain their structure and function. Even though the regulation system of pH is very robust, it can be altered in many diseases, such as cancer, osteoporosis, and diabetes mellitus.[1] Since pH is a metabolic indicator, its accurate measurement can be helpful for diagnostics and therapeutics.

Traditional high-resolution optical imaging techniques, such as confocal microscopy, routinely image pH in cells and tissues by using fluorescent pH-sensitive dyes. However, high-resolution pH images are limited to penetration depths of less than 100 μm, because strong optical scattering in biological tissue blurs the image at greater depths.[2]

Magnetic resonance imaging (MRI) has been employed for *in vivo* pH imaging using either endogenous or exogenous contrast agents, e.g., inorganic phosphate (P_i), intracellular amide proteins, chemical exchange saturation transfer agents, ^{13}C-carbonate, gadolinium-based pH-sensitive contrast agents.[3,4] Generally, the drawbacks include the need of multiple injections to achieve a sufficient contrast agent concentration, relatively low sensitivity, poor spatial resolution, long imaging times, and high cost of performing an MRI. To circumvent some of these disadvantages, a bimodal magnetic resonance-positron emission tomography pH probe has been developed; however, the potential radiation exposure limits its usage.[5]

Address all correspondence to: Lihong Wang, Washington University in St. Louis, Biomedical Engineering, One Brookings Drive, Campus Box 1097, St. Louis, Missouri 63130. Tel: 314-935-6152; Fax: 314-935-7448; E-mail: lhwang@biomed.wustl.edu.

Photoacoustic (PA) sensing of pH has been reported previously in pH sensitive polymeric membranes using a single optical wavelength.[6] Then this method was improved ratiometrically[7] in aqueous solutions of pH sensitive fluorescence dye (SNARF-5F) in clear medium. In this report, for the first time, we demonstrate PA imaging of pH absolute values using linear spectral unmixing at tissue depths of up to 2 mm.

Photoacoustic microscopy (PAM), an emerging biomedical imaging modality for noninvasive *in vivo* studies, has advanced tremendously since its inception.[8,9] In PAM, nonionizing short laser pulses are delivered into a biological tissue. The optical energy is partially absorbed and converted into heat. The heat causes transient thermoelastic expansion, resulting in wideband ultrasound waves which are then detected by an ultrasonic transducer placed outside the tissue.[10] With 100% sensitivity to absorption, PAM can utilize endogenous absorbers such as hemoglobin to produce high-resolution images *in vivo*. Taking advantage of nonradiation optical contrast and low ultrasonic tissue scattering, PAM holds the potential to image pH distribution *in vivo* with high sensitivity and spatial resolution.

Based on the focus mechanisms, PAM has two different implementations (Fig. 1). For optical-resolution photoacoustic microscope (OR-PAM), shown in Fig. 1(a), its lateral resolution (~5 μm) is derived from tight optical focusing by an objective with NA of 0.1.[11] Its axial resolution (~15 μm) is determined by time-resolved acoustic detection, and penetration depth (~700 μm) is similar to other high-resolution optical microscopy techniques.[11] OR-PAM relies on ballistic photons and obeys the penetration limit of one transport mean free path. For acoustic-resolution photoacoustic microscope (AR-PAM) [Fig. 1(b)],[8,9] the fiber-guided laser beam is passed through a conical lens to form a ring-shaped illumination (dark-field), and then focused with the ultrasonic transducer. Because the optical focus is much wider than the acoustic focus, AR-PAM spatial resolutions are mostly determined by the acoustic parameters. Since ultrasound scattering is 2 to 3 orders weaker than optical scattering in biological tissue, an axial resolution of 15 μm and lateral resolution of 45 μm have been achieved with a maximum penetration depth of ~3 mm *in vivo*.[9] Unlike OR-PAM and other optical microscopy techniques, AR-PAM does not rely on ballistic photons. It can provide speckle-free high-resolution structural, functional, and molecular imaging at depths greater than one transport mean-free path in biological tissue.[12–16] Working in different spatial scales, OR-PAM and AR-PAM provide complementary imaging capabilities and can meet the need of various biomedical studies.

In this paper, we report PAM of pH in tissue phantoms, using commercially available SNARF-5F fluorescent dye as the pH-sensitive contrast agent. First, SNARF-5F carboxylic acid stock solution (2.12 mM) was prepared by dissolving 1 mg of SNARF-5F lyophilized powder (Invitrogen, USA) in 1 ml of 50 mM sodium phosphate buffer (pH 6.0). The SNARF-5F stock solution was then diluted to 0.1 mM using sodium phosphate buffers with pH values of 6.78, 7.45, and 7.80, and the final pH values of these diluted SNARF-5F solutions were measured by a commercial pH meter (Thermo Scientific, Florida).

For OR-PAM imaging, the phantom [Fig. 2(a)] was prepared by injecting approximately 80 μl of each of the three 0.1 mM

1083-3668/2011/16(10)/100503/3/$25.00 © 2011 SPIE

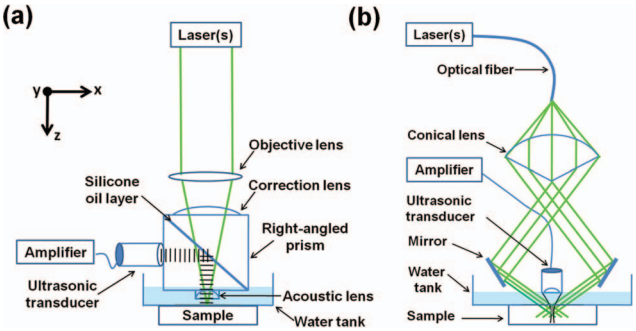

Fig. 1 Schematics of (a) OR-PAM system and (b) AR-PAM system.

SNARF-5F solutions into different Silastic® tube (Dow Corning, USA; inner diameter: 0.3 mm; outer diameter: 0.64 mm). A 2 mm × 3 mm area was raster scanned at optical wavelengths of 581 and 594 nm. The laser repetition rate was set to 1 kHz, and the pulse energy was set to 60 to 80 nJ. The PA signal was calibrated by the reference photodiode signal. To simulate the optical properties of biological tissue, freshly excised nude mouse skin tissue was overlaid on the tubes and the same imaging procedure was repeated.

For AR-PAM imaging, an acrylic phantom with four wells (diameter: 3 mm; center to center distance: 4.5 mm) was machined [Fig. 2(b)]. The left two wells were filled with pH 7.80 SNARF-5F solution, the upper right well was filled with pH 7.45 SNARF-5F solution, and the lower right well was filled with pH 6.8 SNARF-5F solution, respectively. An 11 mm × 13 mm area

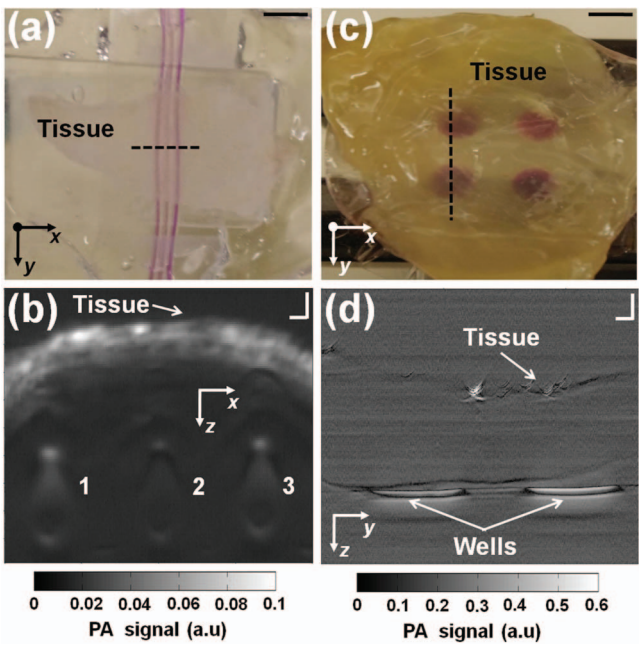

Fig. 2 Photoacoustic microscopy of tissue phantoms with different pH values. (a) Photograph of the tube phantom for OR-PAM with overlaid mouse skin tissue Scalebar: 2 mm. (b) Averaged cross-sectional OR-PAM image of three tubes along the black dotted line in (a). The overlaid mouse skin is ∼200 μm thick Scalebar: 0.1 mm. (c) Photograph of the multiwell tissue phantom for AR-PAM with overlaid chicken breast tissue Scalebar: 4 mm. (d) Averaged cross-sectional AR-PAM image of two wells along the black dotted line in (c). The thickness of breast tissue varied from 1.4 to 2.0 mm Scalebar: 0.5 mm.

was raster scanned at optical wavelengths of 565 and 580 nm. For AR-PAM, the laser repetition rate was set to 1 kHz, and the pulse energy was set to 230 to 300 nJ. The PA signal was calibrated by the reference photodiode signal. Chicken breast tissue was overlaid on the phantom, and the same imaging procedure was repeated.

With the tissue overlay, averaged cross-sectional images, along the black dotted lines in Figs. 2(a) and 2(b), are shown in Figs. 2(c) and 2(d), respectively. For OR-PAM, Fig. 2(c) clearly shows the cross-sections of three tubes overlaid with ∼200 μm thick mouse skin. For AR-PAM, Fig. 2(d) shows the cross-sections of two wells overlaid with chicken breast tissue with the thickness varying from ∼1.4 to ∼2.0 mm. The results demonstrate that PAM can potentially image pH in biological tissue at different depths at least up to 2.0 mm.

Between pH 6.0 and 9.0, the SNARF-5F exists as two distinct populations of acidic and basic forms that have different absorption spectra. The wavelength dependent molar extinction coefficients of each form were calculated from measured spectra. For both OR- and AR-PAM, 300 B-scans were acquired over the scanning area at each optical wavelength, and were converted to maximum amplitude projection images. Pixels within the regions of interest (along the tubes for OR-PAM or inside the wells for AR-PAM) were averaged and segmented from the background. Using spectral unmixing via linear least squares estimation,[9,11,14] the relative concentrations of acidic and basic forms of SNARF-5F were calculated. The ratio of these two concentrations was calculated pixel by pixel and averaged across all pixels within the segmented regions. The final pH image was generated by substituting these ratios into the Henderson–Hasselbalch equation.[1] The absorbance pK_a of SNARF-5F was experimentally determined to be 7.32. For PA imaging with tissue overlays, every three sequential cross-sectional (B-scan) images were averaged, and then pH was calculated as above.

Figures 3(a) and 3(b) show the pH images of the tube phantom by OR-PAM. The calculated pH values along the tubes agree well with those measured by the pH meter. For quantification, an equal number of pixels along the centerline of each tube were selected, where the mean and standard deviation of the pH values were calculated. The pH meter measurements were repeated 6 times for each SNARF-5F buffer solution, and the mean pH value and standard deviation were calculated. The tube areas were segmented based on their physical dimensions in both experiments, and pH was calculated only within the segmented areas. Because the signal-to-noise ratio (SNR) deteriorated by the overlaid skin tissue [Fig. 3(b)], the calculated pH values became less accurate. As a result, the standard deviation of the measured pH in each tube increased by two- to three-fold, yet the mean pH values were still comparable with those given by the pH meter [Fig. 3(e)].

pH images of the multiwell phantom by AR-PAM are shown in Figs. 3(c) and 3(d). Similarly, the well areas were segmented based on their physical dimensions in both experiments, and pH was calculated only within the segmented areas. For quantification, an area containing the same number of pixels was chosen for each well, where the mean pH value and standard deviation were computed [Fig. 3(e)]. The calculated pH values agree well with the pH meter measurements. Similar to OR-PAM, the addition of chicken breast tissue decreased SNR and thus increased the standard deviations of calculated pH results by two-

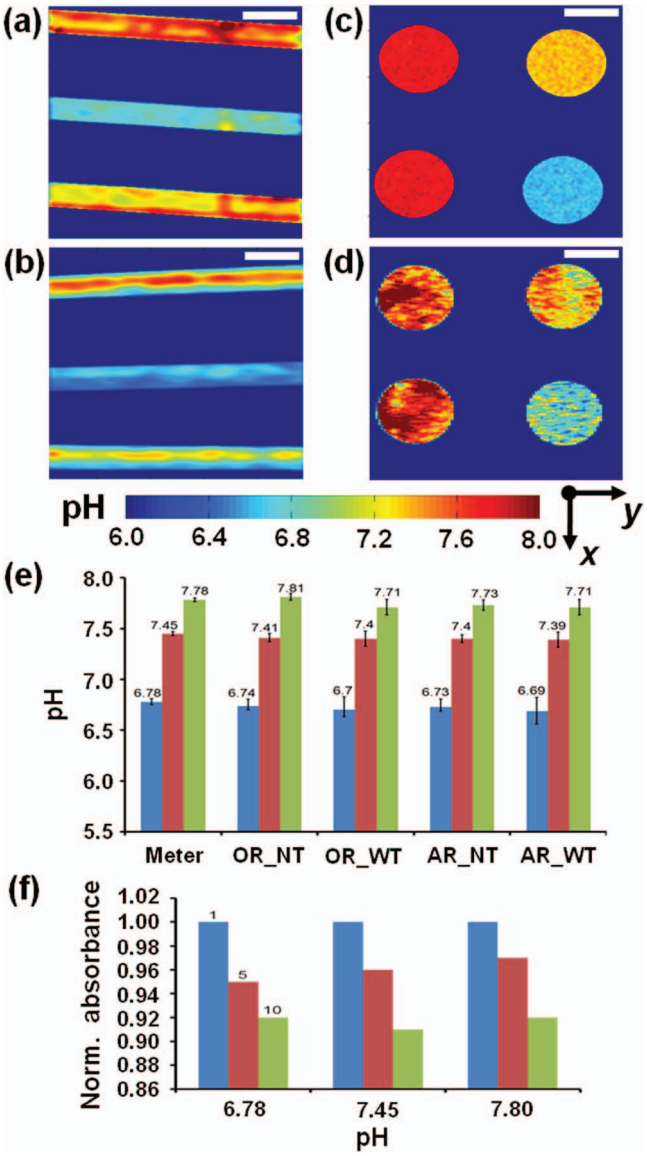

Fig. 3 pH images from OR- and AR-PAM. (a) OR-PAM pH image of three tubes filled with 0.1 mM SNARF solutions with pH of 7.78, 6.78, and 7.45, respectively. (b) OR-PAM pH image of the same phantom with overlaid mouse skin tissue. Scale bar: 1 mm. (c) AR-PAM pH image of four 3-mm diameter wells filled with 0.1 mM SNARF solutions with pH of 7.78, 6.78, and 7.45, respectively. (d) AR-PAM pH image with overlaid chicken breast tissue. Scale bar: 3 mm. (e) Quantitative comparison of pH measurements from pH meter with those from OR- and AR-PAM with and without tissue overlay. The data was shown in mean ± SD. NT: without tissue overlay; WT: with tissue overlay. The correlation coefficients (*R* value) between the pH meter reading and the measurements from OR_NT, OR_WT, AR_NT, and AR_WT were all greater than 0.95 and agree with *p*-values less than 0.05. (f) Normalized mean absorbance at 580 nm of 0.1 mM SNARF buffer solutions with pH 6.78, 7.45, and 7.8 after 1, 5, and 10 PA imaging experiments.

to three-fold. The impact of photobleaching was negligible during both OR- and AR-PAM experiments [Fig. 3(f)]. With storage in darkness and at proper temperature, SNARF-5F solutions are photostable for PA imaging for approximately 1 month.

In conclusion, we have demonstrated the potential of pH imaging using PAM. By two-wavelength PA measurements on OR- or AR-PAM, it was possible to reconstruct the absolute pH values. For both OR- and AR-PAM, the pH measurement accuracy degraded with the increased tissue depth. Additionally, wavelength-dependent optical fluence attenuation may affect the calculation of pH. Future work will extend PA pH imaging to *in vivo* animal studies.

Acknowledgments

The authors thank James Ballard and Sandra Matteucci for help in manuscript edition. This work was supported in part by National Institutes of Health Grant Nos. U54CA136398 and R01 EB000712.

L. V. Wang has a financial interest in Microphotoacoustics, Inc. and Endra, Inc, which, however, did not support this work.

References

1. C. M. Porth, "Disorders of Fluid, Electrolyte and Acid-Base Balance," Chapter 8 in *Essentials of Pathophysiology*, pp. 159–208, Lippincott Williams & Wilkins, Philadelphia (2010).
2. F. Helmchen and W. Denk, "Deep tissue two-photon microscopy," *Nat. Methods* **2**(12), 932–940 (2005).
3. J. Zhou, J. Payen, D. A. Wilson, R. J. Traystman, and P. C. M. van Zijl, "Using the amide proton signals of intracellular proteins and peptides to detect pH in MRI," *Nat. Med.* **9**(8), 1085–1090 (2003).
4. F. A. Gallagher, et al., "Magnetic resonance imaging of pH in vivo using hyperpolarized ^{13}C-labelled bicarbonate,"*Nature (London)* **453**, 940–944 (2008).
5. L. Frullano, C. Catana, T. Benner, A. D. Sherry, and P. Caravan, "Bimodal MR-PET agent for quantitative pH imaging," *Agnew. Chem.* **49**, 2382–2384 (2010).
6. B. Schlageter, et al., "Development of an optoacoustic sensor module for pH and/or CO_2 determination aqueous solutions," *Sens. Actuators B* **38–39**(3), 443–447 (1997).
7. T. D. Hovrath, G. Kim, R. Kopelman, and S. Ashkenazi, "Ratiometric photoacoustic sensing of pH using a 'sonophore'," *Analyst* **133**, 747–749 (2008).
8. K. Maslov, G. Stoica, and L. V. Wang, "In vivo dark-field reflection-mode photoacoustic microscopy," *Opt. Lett.* **30**(6), 625–627 (2005).
9. H. F. Zhang, K. Maslov, G. Stoica, and L. V. Wang, "Functional photoacoustic microscopy for high-resolution and noninvasive in vivo imaging," *Nat. Biotechnol.* **24**, 848–851 (2006).
10. L. V. Wang, "Multiscale photoacoustic microscopy and computed tomography," *Nat. Photonics* **3**(9), 503–509 (2009).
11. K. Maslov, H. F. Zhang, S. Hu, and L. V. Wang, "Optical-resolution photoacoustic microscopy for in vivo imaging of single capillaries," *Opt. Lett.* **33**(9), 929–931 (2008).
12. E. W. Stein, K. Maslov, and L. V. Wang, "Noninvasive, *in vivo* imaging of mouse brain using photoacoustic microscopy," *J. Appl. Phys.* **105**, 102027 (2009).
13. E. W. Stein, K. Maslov, and L. V. Wang, "Noninvasive, in vivo imaging of blood-oxygenation dynamics within the mouse brain using photoacoustic microscopy," *J. Biomed. Opt. Lett.* **14**(2), 020502 (2009).
14. M. Li, J. Oh, X. Xie, G. Ku, W. Wang, C. Li, G. Lungu, G. Stoica, and L. V. Wang, "Simultaneous molecular and hypoxia imaging of brain tumors in vivo using spectroscopic photoacoustic tomography," *Proc. IEEE* **96**, 481–489 (2008).
15. C. P. Favazza, O. Jassim, L. A. Cornelius, and L. V. Wang, "*In vivo* photoacoustic microscopy of human cutaneous microvasculature and a nevus," *J. Biomed. Opt.* **16**(1), 016015 (2011).
16. C. P. Favazza, L. A. Cornelius, and L. V. Wang, "*In vivo* functional photoacoustic microscopy of cutaneous microvasculature in human skin," *J. Biomed. Opt.* **16**(2), 026004 (2011).